ALMA Memo 362

ALMA Receiver Optics Design

J. W. Lamb (Caltech), A. Baryshev (SRON), M. C. Carter (IRAM),
L. R. D'Addario (NRAO), B. N. Ellison (RAL), W. Grammer (NRAO),
B. Lazareff (IRAM), Y. Sekimoto (NRO), C. Y. Tham (U. Cambridge)

2001-Apr-11

CONTENTS

ALMA Receiver Optics Design

J. W. Lamb (Caltech), A. Baryshev (SRON), M. C. Carter (IRAM), L. R. D'Addario (NRAO),
B. N. Ellison (RAL), W. Grammer (NRAO), B. Lazareff (IRAM), Y. Sekimoto (NRO) ,
C. Y. Tham (U. Cambridge)

Abstract— A detailed design for the optical configuration of the ALMA receivers is presented. Individual frequency bands are implemented as self-contained cartridges holding two orthogonally polarized channels. The cartridges are arranged on concentric circles round the center of a 970 mm diameter dewar located on the telescope axis. The beams from them illuminate the secondary mirror through windows on the top of the dewar, either directly or via reflective optics. By having all the beams separate in the focal plane, all bands view the sky simultaneously and selection of the observing band simply requires re-pointing the antenna.

Where possible all the optical elements are integral with the cartridge. For the lowest frequency bands, the optics are too large to go on the cartridge and are located on the top of the dewar. There are no optical elements inside the dewar that are not attached to a cartridge. Since some of the cartridges are far off the telescope axis, mirrors are used to bring the beam closer to the center to reduce aberrations, polarization distortion, and vignetting by the hole in the primary. Provision is made for a mirror to bring the beam of the water vapor radiometer for atmospheric phase correction to the center of the focal plane so it is close to all observing beams.

Several measures are taken to ensure low optical losses: the number of elements is minimized; reflective optics are used where possible; large beam clearances are maintained; and accurate fabrication and alignment tolerances specified. A major driver was to generate minimal cross-polarization, and this was realized by minimizing angles of incidence on offset reflectors, and balancing cross-polarization between consecutive mirrors.

Detailed calculations of the performance, including losses, noise, and polarization have been carried out and are tabulated. There are also estimates of the cryogenic loading. The principal uncertainties are the optimum designs for the vacuum windows and infrared filters.

1 Introduction

Over the last several years there have been various studies of possible configurations for the ALMA receivers [1], [2], [3], [4], [5], [6]. Since the establishment of the Joint Receiver Design Group (JRDG), the requirements have been refined and several major design decisions made, as summarized in Section 2. Principally they prescribe a single dewar for all the receiver bands, and that these bands will be realized as individually testable cartridges. Carter [7] has presented designs embodying some of these concepts but which have required modification in the light of more recent design considerations.

A Workshop was held in Tucson in September 2000 to determine a viable layout for the optics and dewar and this Memo reflects the results, including subsequent refinements. Section 3 lists the design goals for the Workshop, and the configuration that emerged is detailed in Section 4. This includes the overall arrangement, and the details of the optics of the individual bands. These bands were defined by Wootten *et al.* [8] except that Band 1 was subsequently changed from 30–40 GHz to 31.3–45 GHz. They have been endorsed by the ALMA Scientific Advisory Committee (ASAC) [9] with a recommendation to examine the feasibility of extending lower end of Band 3 down to 84 GHz rather than 89 GHz.

The design goals led to a natural division of the bands into three groups. The first category has ambient temperature refractive optics, the second has ambient temperature reflective optics, and the third has cooled reflective optics. Practicable designs for the optics of each of the bands are presented.

While some design changes and improvements will be made later as further study dictates, major changes cannot be implemented without significantly impacting the dewar design, which has been developed in parallel. Thus, it has been necessary to do a detailed design for each of the bands even though only a few will be implemented for initial operation. This will permit bands to be added later with little or no modifications to the dewar. Several elements of the designs are still incomplete, such as precise mixer dimensions and LO injection schemes. During the detailed design phase these may entail some adjustment of the optical parameters also. Nevertheless, the conceptual design presented here has been done in sufficient depth to be confident that a viable final design can be derived from it.

Specific estimates of the expected performance are tabulated for each of the designs. Details for these design calculations are set out in several appendices at the end of the document. These include the aberrations and spillover due to offset feeds, material properties, efficiency calculations, polarization estimates, *etc*.

2   Previous Design Decisions

During the project there have been several major decisions regarding the receiver front-end, which are documented here for reference. Some of these significantly influence the layout of the optics. Major decisions are

1. All cryogenic components will be in a single dewar [10].
2. The cryocooler will provide heat sinks at three temperatures, approximately 70K, 15K, and 4K.
3. Each receiver band (frequency range covered by a pair of orthogonally polarized channels) will be contained in a cartridge, which may be tested as a unit and inserted into the dewar without disturbing any other cartridges [11].
4. The water vapor radiometer (WVR) will be operated in a separate package at ambient temperature [12]. It therefore requires a pick-off mirror to put the beam within 10 arcmin [13] of any of the observing beams.
5. There will be no cold load for receiver calibration. However, provision will be made for a cold load for the water vapor radiometer [14], [15].
6. There will be no quasioptical diplexers for sideband rejection [9]. This is based on a compromise between sensitivity and complexity (reliability).
7. The different bands will share the focal plane so that no switching mirror is required to select a given frequency [14].

These decisions were influenced by both performance criteria and practical considerations. Testability and large-scale production by separate groups dictated that the different receiver bands should be constructed in individual cartridges that can simply be inserted into a single dewar. The major disadvantage of this is that the dewar is larger than it would be with a more integrated approach, but the advantages of being able to change and test individual bands were deemed to be worth this sacrifice.

3   Design Goals

Because of the large number of bands (10 dual-polarization), the wide frequency coverage (> 4 octaves), and the high sensitivity requirements needed to profit fully from the excellent site, the trade-offs among some of the parameters are not straightforward. In

general those parameters which affect most of the observing modes (*e.g.*, sensitivity, reliability) were favored above parameters which were for more specialized modes (such as circular polarization). The physical complexity of the receiver dictated that practical issues had to be seriously considered. These trade-offs are discussed in the text.

The design goals are divided into two categories according to whether they are fundamental to the performance of the receiver, or related to the practicality of construction and maintenance. In some cases there may be conflicts between these goals, but wherever possible the sensitivity should not be compromised.

3.1   Practical Goals

1. Receivers will be interchangeable between antennas (no on site alignment)
2. Optics will be part of receiver — fixed alignment between optics and dewar
3. Antenna mounting flange should be preset within tolerances
4. Cartridges interchangeable between dewars with no re-alignment required
5. Alignment sensitivity to thermal contraction minimized
6. Alignment insensitive to dewar deflections under vacuum
7. Alignment ensured by machining
8. Optics in cartridge where practical
9. Optics cold where practical
10. No moving parts
11. Flexible for future upgrades/clearly defined interfaces
12. Standardize designs among bands
13. Maximize reliability
14. Minimize costs

3.2   Performance Related Goals

1. Minimize window apertures (reduce IR loading and RF loss)
2. Minimize added noise
3. Maximize aperture efficiency: Reduction < 5 %
    a. Aberrations: < 1 %
    b. Truncation loss: < 1 %
    c. Dissipative losses: < 1 %
    d. Scattering losses: < 1 %
    e. Polarization loss: < 1 %
4. Polarization: Beam squint: < 1 % of FWHM[1]

4   Description of Design

The following is a description of the optics including details of the various cartridge optical layouts and the general arrangement of the dewar. As extensive a performance evaluation as possible at this stage of the project is given for each of the designs.

---

[1] This is an extremely demanding goal since it corresponds to 0.005 % cross-polar power.

4.1   General Layout

A dewar with a diameter of about 970 mm will house ten cartridges, one for each of the receiver bands. These cartridges have three stages at the three temperatures provided by the cryocooler. Fiberglass tubes with cutouts are used to stiffly support the stages with minimal thermal conduction. Cartridges are inserted into the base of the dewar, and thermal contact is made to the stages by thermal links that clamp onto the cartridge on cooling [16]. These thermal links are designed not to put any force on the cartridge other than that required for clamping. The cartridge is therefore accurately located by its flange at the dewar wall and the only change on cooling is the shrinkage along its axis. Since this is along the direction of the beam it has a minimal impact on optical performance.

The cartridge concept limits how closely packed the receiver channels may be. However, since the ALMA 12-m antenna[2] has a large field of view [17], excellent performance is still achieved with the feeds widely distributed in the focal plane, provided the higher frequency cartridges are closer to the telescope axis. With the beams separated in the focal plane, a rotating beam selection mirror is not required to bring the observing beam on axis. This simplifies the design and avoids a mechanism susceptible to causing a single-point failure. Section 7.2 presents the details of the aberrations and spillover associated with the off-axis feeds.

At the longer wavelengths the main limitation on the off-axis distance is the size of the hole in the primary mirror. Some of the cartridge radial offsets are large enough that the view of the secondary from the cartridge could be obstructed by the clearance hole in the primary. Consequently, some of the beams need to be brought closer to the telescope axis using reflectors. Conveniently, this turns out not to require any extra optical elements since the bands where it is necessary to translate the beam require an offset ellipsoid and plane mirror pair as part of the optics. The two mirrors can easily be arranged to shift the focal point of the beam to the appropriate position.

Designs for the bands naturally fell into three categories because of the differences in the beam sizes at the various frequencies. For the lowest two bands it is not practical to have reflecting optics since there is insufficient area above the dewar to accommodate the mirrors, and lenses are required. Furthermore, since the beams need to be focused into the dewar to reduce the heat load, the lenses must be at ambient temperature. This type of cartridge is denoted Category A.

Category B comprises the bands for which it was possible to cool some, but not all, of the optics. Some optics must be at ambient temperature since the required size of the optical components does not permit them to fit within the diameter of the cartridge. For practical reasons, it was deemed undesirable to have cryogenic optics attached to the inside of the dewar itself because they are not easily aligned with the cartridge. Bands 3 and 4 fall into this category. In the final implementation it was found that the best scheme required no cold optics.

For Category C cartridges all the optics may be accommodated on the cartridge. This allows all the optics to be aligned and tested as a single unit, which is particularly advantageous for the shorter wavelengths.

---

[2] At the time of writing there has been no final decision on the Atacama Compact Array which would comprise 8-m antennas. Since this has not been defined, the aberration calculations have not been carried out and it cannot be stated what changes to the receiver design would be required.

4.2   Cartridge Designs

Although there are several different designs for the cartridges, they share several common features and design criteria. All the cartridges have a feed horn or quasioptical radiator[3] and one or two focusing elements. These focusing elements are required to image the feed on to the secondary to achieve high efficiency over the whole band, following the concepts presented by Chu [18]. Geometrical Optics is used to obtain the focal parameters and distances for the lenses or ellipsoids, and quasioptical theory is used to determine their sizes and the required clearances. Based on arguments in [19] a clearance diameter of 5 beam radii is initially targeted for all apertures (a beam radius is the $1/e$ amplitude of the best-fit Gaussian beam). This will incur less than 1 % efficiency loss. More detailed examination shows that in some cases the sizes may be reduced. When an aperture or reflector is close to an image of the horn aperture the diameter can be as small as 3.2 beam radii in diameter. At the low frequencies where lenses have to be used, the diameters are decreased to reduce the lens thickness and effect a compromise between dielectric loss and truncation loss.

All the optical trains are designed so that the best-fit Gaussian beam will have an edge taper of 12 dB at the secondary mirror. This will give the highest efficiency when the beam is launched by a corrugated feed horn. When all the higher-order modes are included the actual edge taper will be about 10 dB [19]. Highest efficiency, rather than best G/T (antenna gain over system temperature) has been assumed as the goal since the noise contribution due to diffraction is relatively small. Later some more detailed optimization of the edge taper may be made to improve G/T but only slight improvement can be expected.

Considerable attention has been paid to the polarization purity. Lenses will be anti-reflection treated with polarization-independent layers. Offset ellipsoids are paired to cancel cross-polarization as much as possible, and incidence angles on these mirrors are made as small as is practical. The large beam clearances minimize any polarization effects due to edge diffraction.

Some of the focusing elements also help to reduce the beam size at the entry to the dewar to decrease infrared loading and minimize the vacuum window thickness. This is a particularly important consideration at the longer wavelengths where the vacuum window size would be impractically large.

Some details of the performance calculations are included with the descriptions of the individual bands. Further information on aspects common to all the bands is given in the Appendices.

4.2.1   Cartridge Category A

4.2.1.1   BAND 1 (31.3–45 GHZ) AND BAND 2 (69–90 GHZ)

Bands 1 and Band 2 are the most demanding in terms of size. The optical elements are too large to place in the dewar, so only the feed horns can be cooled. Re-imaging optics are required to achieve reasonable sizes for the horns, and achieve high efficiency that is essentially frequency independent. Two mirrors, one plane and one ellipsoidal, were considered but the folded geometry resulted in optics that were too large to fit in the space above the dewar without obscuring other bands. Using a single lens to couple into the

---

[3] Some bands have two feeds if polarizations are separated quasi-optically. This affects the geometry but the optical design is essentially unchanged.

corrugated horn resulted in a much more compact design. A single feed is used for each band as the polarizations are separated in an orthomode transducer. Since a design had already been developed for the prototype antenna evaluation receiver [20] this was used for Band 1 and scaled down by a factor of two for Band 2. Figure 1 gives the layout and dimensions for the Bands 1 and 2 optics. They comprise a conical corrugated horn and an aspheric PTFE lens. The Band 1 corrugated horn was designed using a mode-matching program to optimize the pattern and the return loss (shown in Figure 2). It has an aperture diameter of 30 mm and an opening angle of 4.57°. To determine the lens focal length and location, a frequency independent quasioptical design was used so that the position of the waist from the horn/lens would match the required antenna waist position. The horn dimensions were halved for Band 2, and the lens was separately optimized.

Although the initial design assumed thin lenses to determine the optical parameter, the final values chosen were based on a more detailed analysis. This included the effect of the thickness of the lens which modifies the amplitude distribution, and the diffraction due to the finite aperture. Since the lens is quite thick it has a significant dielectric loss, and its diameter was chosen to make the loss due to truncation and dissipation roughly the same at 1.5–3 %.

Antireflection layers may be made by machining grooves in the surface. Although circular grooves are the easiest to cut they introduce some cross-polarization and astigmatism [21]. Straight grooves can readily be cut on the flat surface of the lens, but this would be extremely difficult to do on the curved surface. A viable alternative is to drill a regular array of holes into the surface [22], which is proposed for these lenses.
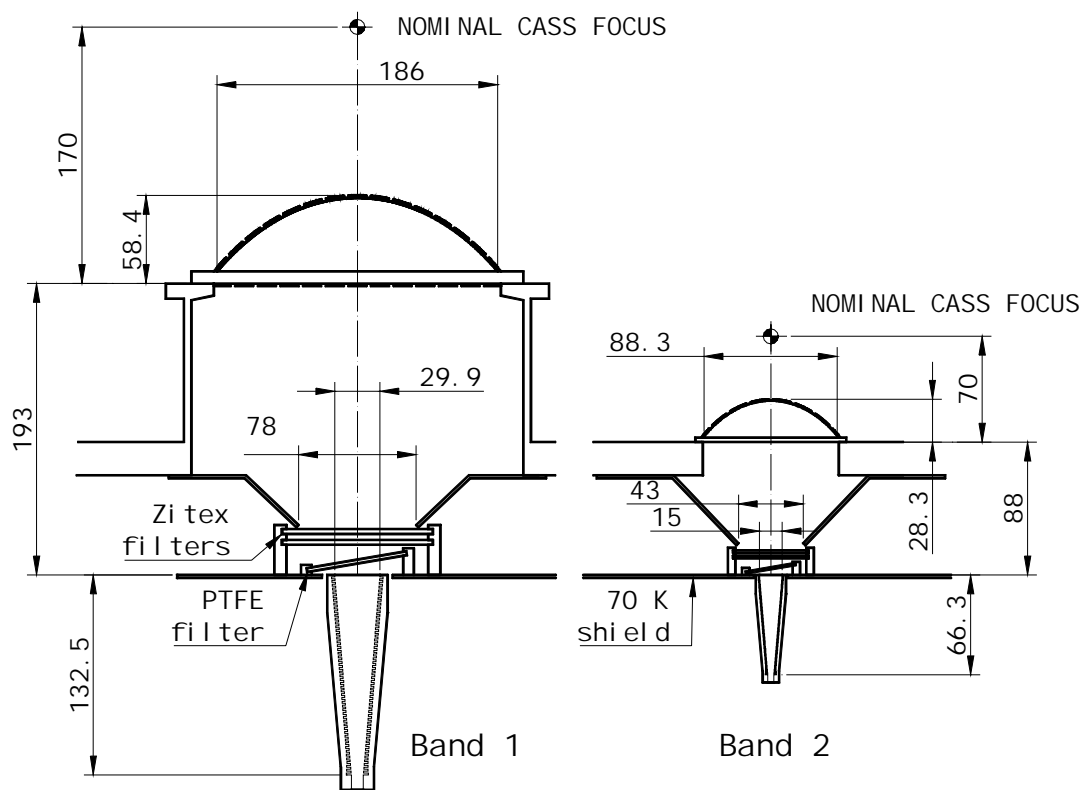

Figure 1. Bands 1 and 2 optical designs. There is a solid PTFE infrared filter attached to the 70 K station and two floating expanded PTFE filters above that.
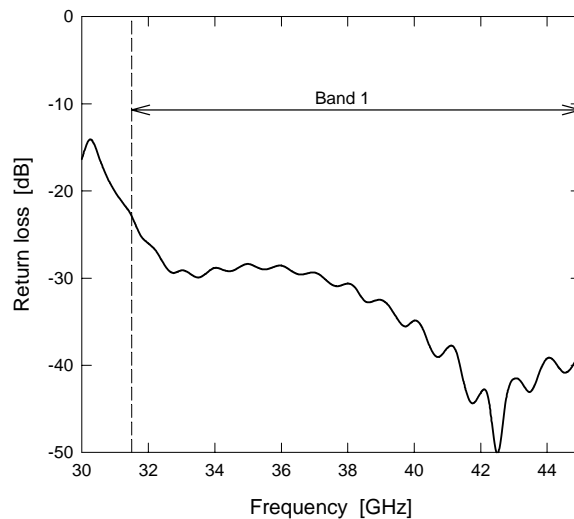
Figure 2. Return loss calculated for Band 1 corrugated horn. The graph for the Band 2 horn is the same scaled by a factor of two on the frequency axis.

The lenses are used as the vacuum window[4], which avoids an extra element in the optics. Since the truncation by the lens is at the level of a couple of percent, care has to be taken that the power not passing through the lens is not reflected back to the horn, resulting in an unacceptable VSWR.

Performance of the optics was determined by calculating the antenna aperture field to find the aperture efficiency. Starting with the horn aperture field determined by mode-matching, the field was propagated to the lens by integration. This field was traced through the lens using ray tracing, and from the lens a diffraction integral used to compute the distribution at the secondary mirror. Most of the contributions to efficiency are therefore directly accounted for, including: departures of the horn aperture field from the ideal $J_0(r)$ distribution; phase errors in the feed aperture; cross-polarization due to the feed; truncation loss at the lens; absorption in the lens ($n = 1.43$, $\tan\delta = 3 \times 10^{-4}$ for Band 1, $\tan\delta = 5 \times 10^{-4}$ for Band 2); and blockage in the aperture plane. Losses which are not included are: reflection, scattering, and absorption in the filters; reflections at the lens surfaces; aberrations at the lens due to the phase center of the wave not being precisely at the focus; and losses due to the offset of the feed from the antenna axis. Separate calculations were used to estimate these contributions.

An infrared filter of PTFE is attached to the 70 K shield [23]. It is two wavelengths thick and has quarter-wave matching layers machined as rectangular grooves on either side (slightly improved performance may be obtained with triangular grooves [24]). Reflections back to the feed are further reduced by tilting the filter by a half-wavelength over the aperture. A set of two floating filters of Zitex reduces the radiation from the window [25]. These are half a wavelength thick and separated by half a wavelength to minimize reflections, and may also need to be tilted to reduce the VSWR. For the PTFE a refractive index of $n = 1.5$, and a loss factor $\tan\delta = 3 \times 10^{-4}$ is taken for Band 1 and $\tan\delta = 5 \times 10^{-4}$ for Band 2 [41]. For the Zitex the same $\tan\delta$ values are used with a refractive index is $n = 1.2$ [26].

---

[4] Since PTFE is known to flow under pressure it may be necessary either to add an HDPE vacuum window at the smallest ambient temperature aperture, or to use HDPE lenses and accept the higher loss.

Table I summarizes the optical performance. Because of the relatively small aperture of the lens, there is a perturbation of the feed pattern at the secondary due to edge diffraction. This appears mainly as a wavelength-dependent phase error that can be removed by refocusing the secondary mirror; this has been accounted for in the Table.

TABLE I

ESTIMATED APERTURE EFFICIENCY LOSS AND ADDED NOISE FOR CATEGORY A CARTRIDGES

Band	Frequency [GHz]	Efficiency Loss [%]	Added Noise [K]
1	31.5	9.9	7.0
	38	6.3	7.1
	45	5.9	8.7
2	67	10.1	10.5
	81	6.9	11.4
	90	8.1	13.5

The two 170 mm diameter cartridges are located on a radius of 295 mm in the dewar. Table I includes the losses due to aberrations resulting from the lateral offset of the feeds in the focal plane. The feeds and lenses are tilted to point at the center of the secondary mirror (though this is not explicitly illustrated in Figure 1).

4.2.2 Cartridge Category B

4.2.2.1 BAND 3 (84–116 GHZ) AND BAND 4 (125–164 GHZ)

Band 3 and Band 4 are both Category B bands (Figure 3). Again, these have single corrugated feed horns with orthomode transducers in waveguide. The antenna beam is focused down using an offset ellipsoid to reduce the window diameter and infrared loading. Several designs using one or more lenses or reflectors inside the dewar were investigated but these resulted in impractically thick lenses or awkward geometries. By using as large a horn as practical and moving it up close to the dewar wall an acceptable solution was obtained. Both bands are housed in 140 mm diameter cartridges.

In Band 3 a plane mirror reflects the incoming beam through an angle of 52° to the offset ellipsoidal mirror with a focal length of 149 mm. The ellipsoid redirects the beam down through a 50° angle to the feed horn. This feed has an aperture of 24 mm and a length of 140 mm. This combination produces a frequency-independent illumination of the secondary mirror.

One of the less desirable features of this design is the limited volume for infrared filtering, but a polystyrene foam block makes a reasonably effective block with low loss at millimeter wavelengths. At these wavelengths the scattering of foam dielectrics is much less than 1 %.

For Band 4 a similar design was used with the same optical parameters. However, because of the narrower beam, a smaller mirror can be used and the angle of incidence on the offset ellipsoid reduced from 25° to 20° with a consequent reduction in cross-polarization.

Two types of window were considered. Films of PETP (Mylar or Melinex) have been used in millimeter and sub-millimeter receivers but the thin films required to minimize reflections have significant permeability to water. Even a thickness of only 50 μm has a

significant reflection at these wavelengths. By using two layers separated by about quarter of a wavelength this reflection can be reduced to an acceptable level. However, this relies on keeping the films parallel which is difficult if the inner film is under vacuum. The foam IR filter can support it, but some gradual deformation may be expected over time and the performance will be correspondingly degraded. It is possible that dry gas could be circulated between the two films to reduce water infusion, but this adds undesirable complexity.

An alternative is to use HDPE windows that are one (electrical) wavelength thick and have antireflection grooves on both sides (rectangular or triangular). This turns out to be a better solution with lower reflection and dissipation losses since PETP has a high dielectric constant and loss ($n = 3.35$, $\tan\delta = 100 \times 10^{-4}$ [27]). The reflection loss of the HDPE window is <0.3 % and the dissipation loss is <0.6 %.

Table II lists the expected performance measures for Category B cartridges.

Figure 3. Layout and dimensions for Bands 3 and 4 optics.

TABLE II

ESTIMATED APERTURE EFFICIENCY LOSS AND ADDED NOISE FOR CATEGORY B CARTRIDGES

Band	Frequency [GHz]	Efficiency Loss [%]	Added Noise [K]
3	84	2.8	5.3
	100	2.4	5.0
	116	2.3	4.6
4	125	2.7	5.6
	144	2.4	4.9
	163	2.6	5.1

4.2.3   Cartridge Category C

Category C cartridges comprise Bands 5–10. Internally, the optics vary among the cartridges according to the specific constraints of the bands, but they share many common features[5]. For all the bands the nominal antenna secondary focus is close to the top of the dewar. Imaging of the beam is done by cold reflective optics with two mirrors. Corrugated horns are the preferred beam-forming elements, but 'planar' structures such as twin-slot antennas on hyper-hemispherical lenses may be considered for the upper frequencies. For the higher frequencies quasioptical polarizers and LO injection components will also be required.

4.2.3.1   BAND 5 (165–211 GHZ) AND BAND 6 (211–275 GHZ)

Optical layouts for Band 5 and Band 6 are shown schematically in Figure 4. Each band has a single corrugated feed, and waveguide couplers and orthomode transducers are used for LO injection and polarization separation respectively. Two offset ellipsoids couple the beam to the secondary and the relative orientations of the mirrors result in partial cancellation of the cross-polarization.

As for Bands 1 and 2, there are solid PTFE IR filters on the 70 K shield, and a pair of floating Zitex filters above. It is assumed that the solid PTFE filters are three and four half-wavelengths thick for the two bands respectively ($n = 1.5$, $\tan\delta = 3 \times 10^{-4}$). The Zitex filters are two half-wavelength sheets separated by half a wavelength ($n = 1.2$, $\tan\delta = 3 \times 10^{-4}$). The vacuum windows are HDPE, 6 and 8 half-wavelengths thick (3.16 mm and 3.24 mm) for the two bands. Dielectric parameters $n = 1.524$ and $\tan\delta = 3 \times 10^{-4}$ were taken in both cases.
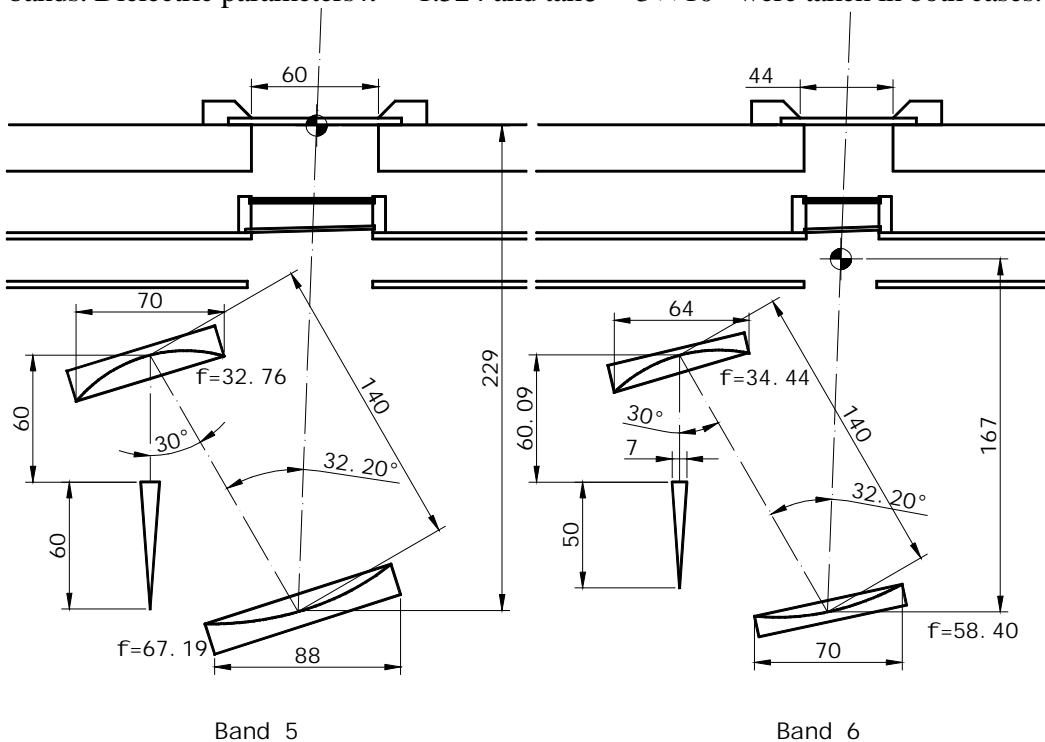

Figure 4. Layout and dimensions for Band 5 and Band 6 optics.

---

[5] Interestingly, there was a convergence among three different groups to designs that were very similar in principle, differing only in some of the details.

4.2.3.2   BAND 7 (275 GHZ–370 GHZ)

For Band 7 frequencies (and higher), a quasi-optical polarization diplexer is more appropriate than any of the waveguide orthomode transducers that have been studied because of the complexity of fabrication. Two separate mixers and feeds are therefore required. Waveguide LO injection is practical for Band 7, however, and experience with IRAM receivers shows that receiver stability is better than for systems with quasi-optically injected LO. From the perspective of losses and matching LO power, it is advantageous to have the two mixers close together, which sets constraints on the arrangement of the optical elements.

As represented in Figure 5, there are two mixers with their axes parallel and separated by 43 mm. Each has an offset ellipsoid that refocuses the beam to a waist near the polarizing grid. A second ellipsoid then matches the beam to the telescope. The cross-polar power from the first ellipsoid, which is only about 0.3 %, is terminated at the other port of the grid, and there is therefore no possibility of cancellation of this at the second ellipsoid. However, by using a small angle of incidence (12.5°) and a long focal length (76 mm) the amount of cross-polarized power generated by this element is kept to an acceptably low level. The power in the cross-polar component is ~0.018 % with an associated 2.6 % beam squint between the orthogonal circular polarizations.
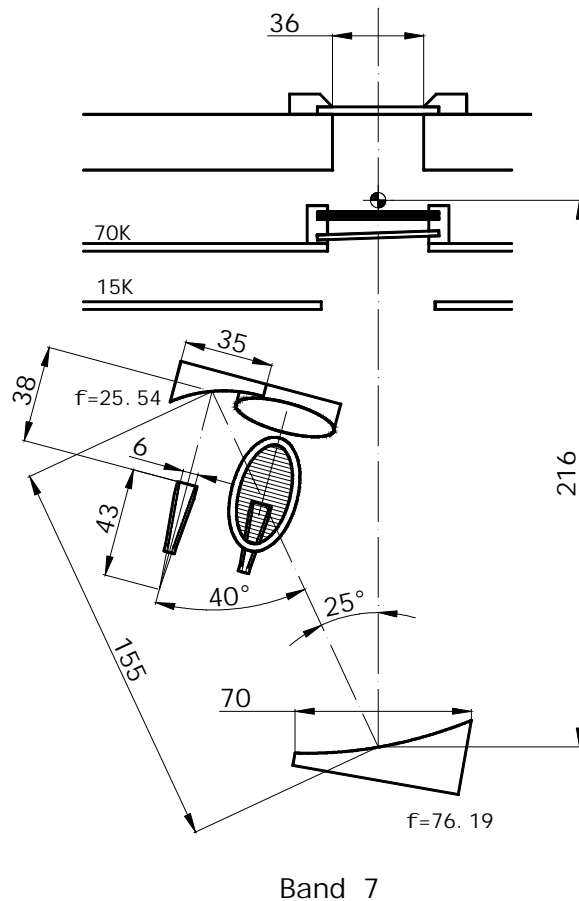

Band 7

Figure 5. Schematic of the Band 7 optics configuration.

For IR filtering there are a solid, grooved PTFE filter, two wavelengths thick (1.24 mm), on the 70 K station, and two half-wavelength thick (0.38 mm) Zitex sheets as a floating shield above. Vacuum window loss calculations assume an HDPE vacuum window 10 half-wavelengths thick at mid-band (3.05 mm) with quarter-wave anti-reflection grooves. A wire grid polarizer with 10 μm diameter wires separated by 40 μm should have approximately equal leakage for the two polarizations [28]. Results of the overall performance are shown in Table III.

4.2.3.3   *BAND 8 (385–500 GHZ) AND BAND 10 (787–950 GHZ)*

Band 8 and Band 10 designs are based on the design for the Japanese ASTE telescope [29]. There is a separate corrugated feed horn for each polarization and these are combined at a wire grid (Figure 6). Two offset ellipsoids match the beams from the feeds to the telescope and are arranged to have a significant cancellation of the cross-polarization. The horn for Band 8 is an optimum gain design (*i.e.*, the shortest horn for a given beamwidth), and the Band 10 horn is essentially the same size. LO power is coupled in through the spare port of the wire grid used to separate the two polarizations.

Zitex filters are suitable for IR blocking. In this frequency range the loss of solid PTFE is increasing, but sheets of Zitex, which are thick enough to be IR blocks, are still reasonably transparent even in the sub-millimeter. Benford *et al.* [26] give an empirical equation for the absorption coefficient, which is applicable above 300 GHz or so. From those data we derive $n = 1.22$ and $\tan\delta = 1.8 \times 10^{-4}$ for Band 8 and $n = 1.22$ and $\tan\delta = 7.3 \times 10^{-4}$ for Band 10. Thicknesses are 3 half wavelengths for the sheet on the 70 K shield and one half wavelength for the two sheets above. These correspond to 0.34 mm and 0.83 mm for Band 8 , and 0.17 mm and 0.42 mm for Band 10. HDPE is still sufficiently transparent to use as a vacuum window [30]. A 10 half-wavelength window for Band 8 is 2.22 mm thick, and a 15 half-wavelength window for Band 10 is 1.7 mm. At these frequencies $n = 1.524$ and $\tan\delta = 4 \times 10^{-4}$ for Band 8 and $n = 1.524$ and $\tan\delta = 6.3 \times 10^{-4}$ for Band 10.

Figure 6. Band 8 and 10 layouts. The LO is injected at the polarizing grid.

There is also an option to make these two bands with a single offset ellipsoid each [31]. This would increase the distortion and cross-polarization losses slightly, but the amount of cross-polar generated in the aperture could be minimized by inserting the polarization diplexing grid in between the ellipsoid and the secondary mirror.

4.2.3.4   *BAND 9 (602—720 GHZ)*

Band 9 optics [32] are partially based on the optical design by van de Stadt for the FIRST HIFI receiver [33]. The original design comprised two ellipsoidal (converging) mirrors with an intermediate hyperboloidal (diverging) mirror. In adapting this design for the ALMA receivers, it was found that frequency independence and suppression of cross-polar components (at the band center) could be achieved with just two ellipsoids, if the angles of incidence are correctly chosen. The resulting layout is similar to that of Bands 8 and 10.

Figure 7. Optical scheme for Band 9 using offset ellipsoids designed for distortion compensation.

Several types of feed for the signal are being considered, including waveguide corrugated horns and quasi-optical antenna/lens combinations. Both types can be matched to the telescope beam with the two-mirror combination that fits in the same space envelope. The layout depicted in Figure 7 uses an optimum gain corrugated horn. Both quasi-optical balanced and waveguide balanced schemes are contemplated. The signal path optics will stay the same in either case.

LO injection in this band will be done quasi-optically. LO coupling through thin Mylar film beamsplitters with coupling between –10 dB and –20 dB is being considered for the single-ended mixers. For the quasi-optical balanced configuration a polarization separation grid will be used for LO injection. For waveguide balanced mixers LO will be injected individually into each mixer through the LO ports.

For these estimates the vacuum window was taken to be made from HDPE ($n = 1.524$ and $\tan\delta = 4 \times 10^{-4}$) 10 half-wavelengths thick, or 1.49 mm. The filters were a single Zitex sheet half a wavelength thick (0.327 mm) at the 15 K shield and two one wavelength thick sheets at the 70 K shield. Relevant dielectric parameters were $n = 1.22$ and $\tan\delta = 4 \times 10^{-4}$.

For Bands 5–10 the expected performance measures are listed in Table III.

TABLE III

ESTIMATED APERTURE EFFICIENCY LOSS AND ADDED NOISE FOR CATEGORY C CARTRIDGES

Band	Frequency [GHz]	Efficiency Loss [%]	Added Noise [K]
5	163	5.0	3.1
	187	2.4	2.5
	211	5.0	3.8
6	211	6.4	4.9
	243	3.5	3.5
	275	5.7	5.2
7	275	7.0	5.7
	323	5.1	6.0
	370	6.9	7.6
8	385	10.5	5.5
	442	6.0	5.1
	500	11.0	6.7
9	602	9.7	6.7
	661	7.7	6.6
	720	10.8	8.0
10	787	13.7	11.7
	868	11.4	12.6
	950	16.1	14.7

4.3   Summary of Optical Parameters

The values of the optical parameters (defined in Figure 8) for all the bands are summarized in Table IV.
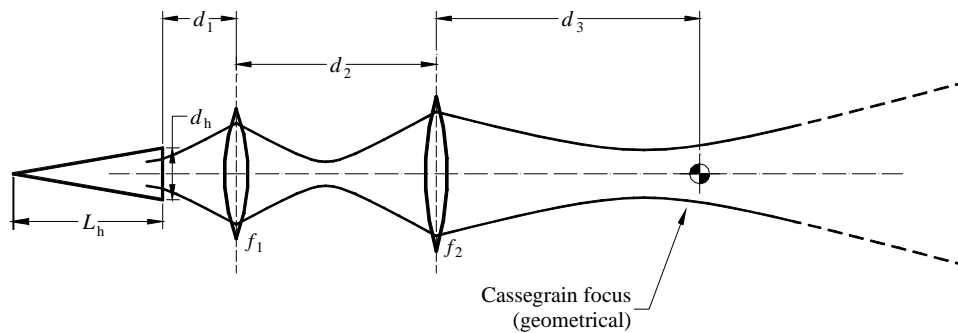

Figure 8. Geometrical parameters used for the optics. Bands 1–4 have only one focusing element represented by lens 1.

Parameters for the ellipsoidal reflectors used in Bands 3–10 are given in Table V along with the effective surface error contribution of the aberrations resulting from the frequency dependent phase center positions of the beams.

TABLE IV

OPTICAL PARAMETERS FOR BANDS 1 TO 10

Parameter	Band									
	1	2	3	4	5	6	7	8	9	10
d_h	30.00	15.00	24.00	24.00	9.00	7.00	6.00	8.69	4.22	8.06
L_h	180.52	90.26	140.00	140.00	60.00	50.00	43.00	35.29	12.87	26.77
d_1	193.00	88.00	152.70	152.70	60.05	59.89	38.00	90.00	41.79	82.00
f_1	188.00	88.00	149.08	149.08	32.76	34.44	25.53	41.79	28.43	35.31
d_2	–	–	–	–	140.00	140.00	155.00	125.00	82.33	100.00
f_2	–	–	–	–	67.19	58.40	76.19	46.65	25.62	37.77
d_3	170.00	70.00	303.85	303.85	229.84	166.86	216.00	186.00	100.00	181.00

TABLE V

PARAMETERS FOR THE OFFSET ELLIPSOIDS. f_1 IS THE EFFECTIVE FOCAL LENGTH AND r_{s1} AND r_{s2} ARE THE SOURCE AND IMAGE RADII OF CURVATURE FOR MIRROR 1, WITH CORRESPONDING PARAMETERS FOR MIRROR 2. θ_{ref} IS THE ANGLE BETWEEN INPUT AND OUTPUT BEAMS, ν_{min} AND ν_{max} ARE THE LOWER AND UPPER FREQUENCIES IN THE BAND, AND ε_{eff} IS THE CORRESPONDING EFFECTIVE SURFACE ERROR FOR THE ABERRATION. FOCAL LENGTHS ARE IN MILLIMETERS, SURFACE ERRORS IN MICRONS, AND ANGLES IN DEGREES.

	Band							
	3	4	5	6	7	8	9	10
Mirror 1								
f_1	149.08	149.08	32.76	34.44	25.53	41.79	28.43	35.31
r_{s1}	190.75	214.06	67.78	65.28	44.54	110.88	64.15	105.379
r_{i2}	682.55	491.13	63.39	72.91	59.85	67.07	51.06	53.31
θ_{ref}	50	40	30	30	40	30	49.5	30
ν_{min}	84	125	163	211	275	385	602	787
ε_{eff}	13.5	4.4	5.6	3.6	4.4	2.0	1.9	0.5
ν_{max}	116	163	211	275	370	500	720	950
ε_{eff}	8.3	3.1	3.7	2.4	2.6	1.4	1.9	0.4
Mirror 2								37.770
f_2	–	–	67.19	58.40	76.19	46.65	25.62	47.151
r_{s2}	–	–	81.82	73.42	106.26	59.32	32.13	189.847
r_{i2}	–	–	375.82	275.4	269.2	218.5	126.546	31.1
θ_{ref}	–	–	32.05	32.5	25	31.1	60	
ν_{min}	–	–	163	211	275	385	602	787
ε_{eff}	–	–	12.4	2.0	1.0	1.4	1.5	0.3
ν_{max}	–	–	211	275	370	500	720	950
ε_{eff}	–	–	8.7	2.3	1.4	1.0	1.2	0.3

4.4   Circular Polarization Beam Squint

Exact calculations of the beam squint between orthogonal polarizations have not yet been made but some simple estimates are tabulated below. For optical trains with two offset ellipsoids the magnitude of the cross-polar has been taken as the difference between the cross-polar for the individual ellipsoids. The orientations of the mirrors are appropriate for polarization cancellation in the geometrical optics limit. In the quasioptical regime the distance between the mirrors is an important factor also, but the appropriate parameter (the 'phase-slippage') has not been evaluated. The actual cancellation may be less than assumed, especially at the lower frequencies (see Section 7.1.5). The total for the receiver optics plus antenna optics is estimated as the root-sum-of squares since the high-order cross-polar modes generated by the optics will probably add in quadrature with the modes from the antenna [19].

TABLE VI

ESTIMATED BEAMSQUINT BETWEEN LEFT AND RIGHT CIRCULAR POLARIZATIONS.

Band	Frequency [GHz]	Optics [%]	Antenna [%]	Estimated Total [%]
1	31	–	2.6	2.6
	38	–	2.6	2.6
	45	–	2.6	2.6
2	67	–	2.6	2.6
	78	–	2.6	2.6
	90	–	2.6	2.6
3	84	0.6	1.8	1.9
	100	0.5	1.8	1.9
	116	0.2	1.8	1.8
4	125	0.4	1.8	1.8
	144	0.4	1.8	1.8
	163	0.3	1.8	1.8
5	163	0.3	2.5	2.5
	187	0.2	2.5	2.5
	211	0.2	2.5	2.5
6	211	0.3	2.5	2.5
	243	0.2	2.5	2.5
	275	0.0	2.5	2.5
7	275	0.6	1.0	1.2
	323	0.3	1.0	1.0
	370	0.3	1.0	1.0
8	385	0.1	1.0	1.0
	442	0.1	1.0	1.0
	500	0.1	1.0	1.0
9	602	0.2	1.0	1.0
	661	0.1	1.0	1.0
	720	0.1	1.0	1.0
10	787	0.1	1.0	1.0

4.5   Dewar Layout

The dewar layout is defined largely by the diameters of the cartridges. Those were chosen to be 170 mm for Bands 1, 2, and 5–10 and 140 mm for Bands 3 and 4, based on preliminary designs for some of the bands [34]. Taking into account these diameters as well as allowances for the flanges and thermal links [16], led to a dewar with a diameter of 970 mm and cartridges located at diameters of 300 mm, 590 mm, and 670 mm.

The arrangement of cartridges is presented in Figure 9. The coordinate system has the *x*-axis parallel to the antenna elevation axis, the *y*-axis away from the cabin door (*i.e.,* down when the antenna is in the horizon position), and the *z*-axis in the antenna boresight direction. This is in accord with the antenna reflector coordinate system [35].
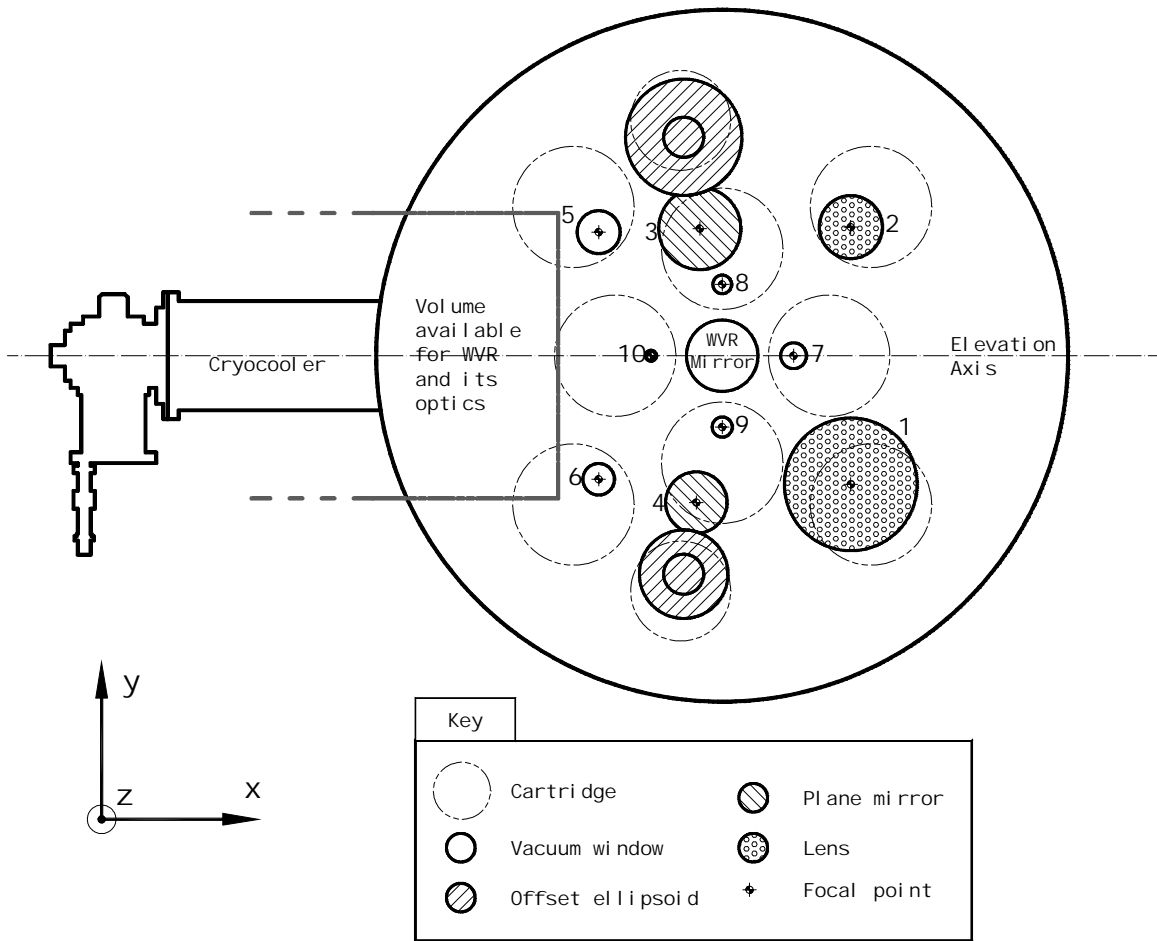
Figure 9. Layout of the dewar viewed from the top. The optics for the WVR are not defined yet, but the central pickoff mirror shown should be large enough should it be necessary to implement refraction correction.

TABLE VII

DIMENSIONS AND LOCATIONS OF CARTRIDGES AND BEAMS IN THE DEWAR. THE DEFOCUS LOSS IS THE RESIDUAL LOSS AFTER MOVING THE SECONDARY MIRROR TO THE OPTIMUM LOCATION. THE TOTAL DEFOCUS BEFORE CORRECTING IS THE DISTANCE OF THE OPTICS FOCAL POINT RELATIVE TO THE PETZVAL SURFACE. THE NOMINAL FOCUS IS ON THE TOP OF THE DEWAR.

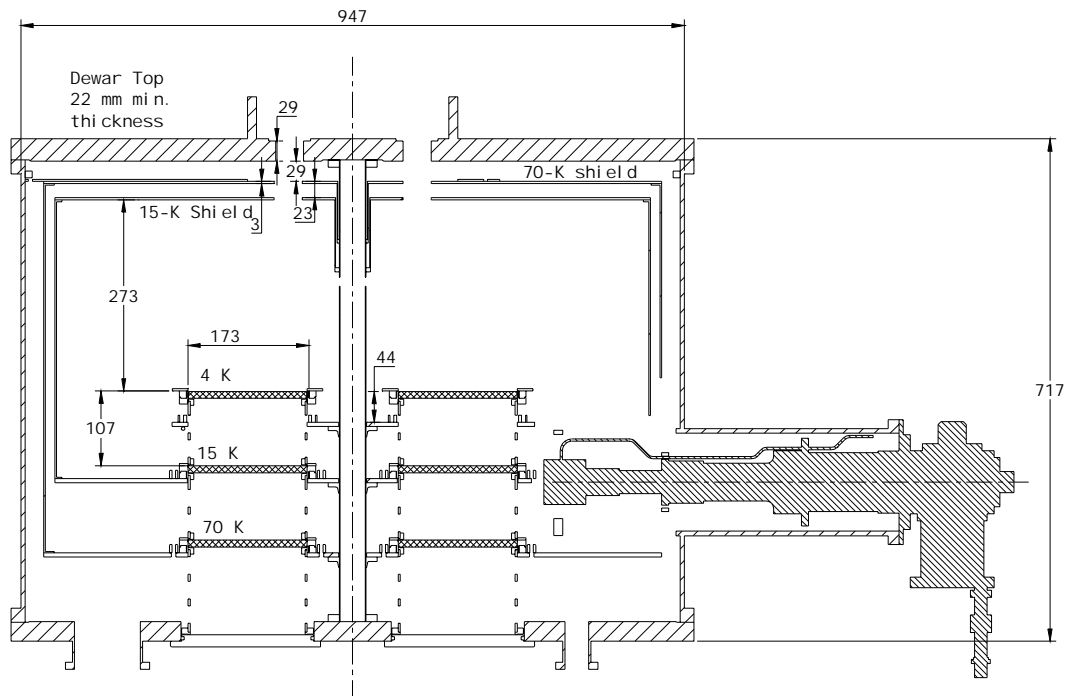| Band	Cartridge Diameter [mm]	Cartridge Radial Location [mm]	Cartridge Azimuth [deg]	Beam Radial Location [mm]	Focus Location Above Dewar [mm]	Petzval Distance [mm]	Total Focus [mm]	Mid-band Frequency [GHz]	Defocus Loss [%]
1	170	295	-45	255	275	145.0	130	38	0.003
2	170	295	45	255	70	145.0	-75	78	0.004
3	140	335	100	181	182	187.0	-5	100	0.000
4	140	335	-100	181	178	187.0	-9	144	0.000
5	170	295	135	245	0	145.0	-145	187	0.077
6	170	295	-135	245	-63	145.0	-208	243	0.267
7	170	150	0	100	-19	37.5	-57	323	0.035
8	170	150	90	100	-11	37.5	-49	442	0.048
9	170	150	-90	100	-39	37.5	-77	661	0.267
10	170	150	180	100	5	37.5	-33	868	0.083

Figure 10. Section through cartridge showing main features and dimensions.

4.6   Infrared Loading

Estimates of the thermal loading on the cryocooler are based on various previous measurements [36], [23], [25], and further investigations are underway in an ALMA work package [37]. The present best estimates given in Table VIII are based on [6].

TABLE VIII

ESTIMATED LOADING ON THE CRYOCOOLER FROM THE VACUUM WINDOWS AND INFRARED FILTERS

Band	Window area [mm²]	Filter 1 area [mm²]	Filter 2 area [mm²]	IR Radiation [W]	Load on 1st stage [W]	Load on 2nd stage [W]	Load on 3rd stage [W]
1	4 778	1 662	-	2.19	1.096	0.038	-
2	1 452	380	-	0.67	0.333	0.009	-
3	2 463	1 018	-	1.13	0.565	-	0.023
4	2 463	1 018	-	1.13	0.565	-	0.023
5	2 827	2 827	2 552	1.30	0.648	-	0.059
6	2 827	908	908	1.30	0.648	-	0.021
7	962	1 590	1 257	0.44	0.221	-	0.029
8	616	755	573	0.28	0.141	-	0.013
9	254	755	573	0.12	0.058	-	0.013
10	177	755	573	0.08	0.041	-	0.013
Totals	18 820	11 668	6 434	8.63	4.316	0.047	0.194

4.7   Water Vapor Radiometer

The water vapor radiometer will be a self-contained unit with a pickoff mirror on the axis of the cryostat. This puts the WVR beam within 10 arcmin of any of the observing beams. By rotating the pickoff mirror continuously about an axis slightly inclined to the mirror normal, the beam may be scanned round the antenna aperture to obtain information for atmospheric refraction correction [38]. This requires a mirror that is about twice the size of the mirror that would be used to fully illuminate the aperture, so sufficient space has been allocated for this. Note that the WVR beam can pass over the windows for other bands without problem.

No details of the optics for the WVR are given here apart from the central pick-off mirror. These will be separately determined by the groups responsible for those responsible for the instruments.

4.8   Optical Devices Above Dewar

A sufficient volume has been allocated above the dewar (Figure 11) for various optical devices. At present these 'widgets' are undefined but could include some or all of the following:

1.   An ambient temperature absorber for calibration
2.   A partially transparent vane for calibration
3.   One or more quarter-wave plates for producing circular polarization
4.   A grid for cross-calibration of orthogonal linear polarizations
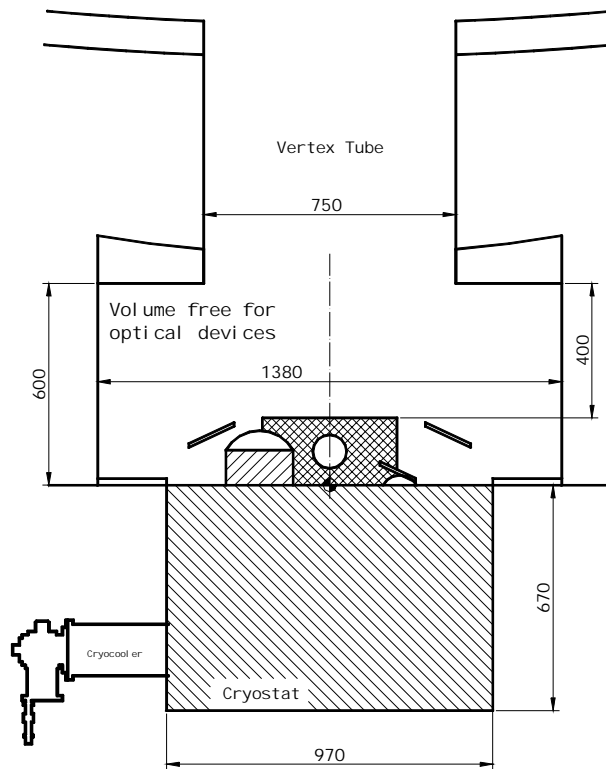5.   A solar attenuator

Figure 11. Arrangement of cryostat in receiver cabin, showing space available for any required optical devices.

5   Conclusions

A very practical design for the ALMA Front End package has been developed as far as the optics and dewar are concerned. All bands are be implemented as cartridges that will be built and tested individually. By arranging the beams appropriately in the focal plane the need for a rotating selection mirror is avoided with negligible impact on performance. All the bands feature low-loss and wide bandwidths, apart from Bands 1 and 2 for which the long wavelengths forced moderate compromises in sensitivity. Particular attention was paid to achieving low cross-polarization.

For the most part the goals stated in Section 3 have been met. The primary exceptions are the efficiency at the highest and lowest bands, and the circular polarization beam-squint. Some minor improvements may be made in both areas, but in fact the results are already very good. A more complete analysis needs to be made of the polarization performance since the methods used here have been rather approximate. In particular the detailed interaction between the effects of the individual ellipsoids and the feed offset in the Cassegrain antenna must be quantified. Minor optimization of the antenna edge taper should also be made on a band-by-band basis.

Finally, the vacuum window and IR filter designs need to be thoroughly verified for their IR and mm/sub-mm performance.

6   Acknowledgements

Many people have contributed to the work described in this document, and we would particularly like to thank: Mark Harman, Stéphane Claude, and Doris Maier. We would also like to thank John Payne and Darrel Emerson for reviewing the results at the Tucson meeting, and Eric Lepie ("*Eric's Ice Cream*") for providing nutritional support.

7   Appendices

7.1   Basis for Performance Calculations

To maintain some consistency in the evaluation of performance calculations, a common set of parameters was used for the different designs. These are stated below, and further information may be found in [19].

7.1.1   Ohmic Losses in Metallic Reflectors and Grids

Losses in metals depend on the material, surface treatment, and temperature. To be as realistic as possible the loss estimates were based on results of carefully calibrated measurements by Gatesman *et al.* at 584 GHz [39]. For aluminum they obtain a reflection loss of 0.5 % and for copper 0.3 %. We will assume that the mirrors will be aluminum, though copper plating may be considered for the room temperature reflectors. Although there should be a dependence on the angle of incidence [40], this is small enough for the materials and angles involved to ignore. For frequency dependence we take a square-root dependence, so that for room temperature reflectors we get a loss[6] L given by

$$1 - L^{-1} = 0.5 \sqrt{\frac{f}{584 \text{GHz}}} \% \tag{1}$$

At lower temperatures the conductivity will increase by some factor depending on the temperature, the material, and the preparation. Since the cryogenic mirrors will be operating at < 10 K the thermal noise emitted by them will be completely negligible. Similarly, the efficiency loss will be very small, and we shall just assume half the room temperature loss as being a sufficiently good estimate.

7.1.2   Dielectric Losses

Large variations in material parameters make it difficult to estimate the losses in dielectric materials used for lenses, filters, and windows [41]. The best materials appear to be PTFE for frequencies up to about 200 GHz, having a loss tangent around 4×10^{-4} [30], and HDPE for higher frequencies, with a loss tangent $< 6 \times 10^{-4}$ up to 900 GHz [42]. For the different bands representative values from the literature were used. In the receiver construction phase all optical dielectrics will need to be measured to verify the dielectric constant and low loss, as well as material integrity (homogeneity, cracks, bubbles, inclusions, *etc*.).

7.1.3   Ruze Loss

Scattering due to surface inaccuracies is accounted for by the distortion of the wavefront. For a reflector with an rms deviation of the surface of ε_r the loss at a wavelength λ is

---

[6] Loss is defined as incident power over transmitted (or reflected) power.

$$1 - L^{-1} = \exp\left(-\left(\frac{4\pi\varepsilon_r}{\lambda}\right)^2\right) \tag{2}$$

A lens with a surface accuracy of ε_l has a loss per surface of

$$1 - L^{-1} = \exp\left(-\left(\frac{2\pi\varepsilon_l}{\lambda}(n-1)\right)^2\right) \tag{3}$$

which has to be doubled for two surfaces.

The machining accuracy requirement will depend on the wavelength. At higher frequencies the optical components will be smaller and therefore easier to machine to the higher tolerances. Metallic reflectors can be machined to higher accuracy than softer dielectrics, but this is compensated by the less stringent tolerance requirements for dielectrics. For the calculations we assume an accuracy of 5 µm for mirrors and 15 µm for lenses at frequencies below 370 GHz. At higher frequencies we take 3 µm and 8 µm respectively.

Since the corresponding added noise depends on where the scattered power is terminated, we make some simple assumptions. Errors on a large scale will scatter power close to the nominal direction of the beam, and because of the relatively large beam clearances of the optics it will be terminated mainly on the sky. Small scale errors will scatter power out of the optics: for the cryogenic optics we will assume a termination of 70 K and for the ambient it will be 290 K. Furthermore, we will assume that half the surface error is small scale, leading to an ambient temperature contribution, and half is large scale, leading to a sky contribution.

7.1.4 Truncation Loss

When a beam is truncated there are two types of loss: the power that is stopped by the aperture and the power that is scattered (diffracted). For small losses, these two are approximately equal [19]. Hence, if a beam is vignetted such that –20 dB of the power is intercepted by the stop, then the loss will be ~2 %, half on each side of the aperture. The added noise should be calculated taking into account where the stopped (absorbed or reflected) and diffracted power will to be terminated.

For this memo all the optical systems were evaluated using a scalar diffraction integral to estimate the fields at all of the apertures. This gives some idea of the cumulative effects of consecutive stops.

7.1.5 Cross-Polarization and Distortion at Offset Mirrors

Offset mirrors generate cross-polarization and distortion of the optical beam. Murphy [43] has analyzed these effects for a Gaussian beam and found that the power scattered out of the fundamental mode into higher-order modes (*i.e.*, amplitude distortion) is

$$1 - L_d^{-1} = \frac{1}{8}\left(\frac{w}{f}\right)^2 \tan^2(i) \tag{4}$$

where w is the beam radius at the mirror, i is the angle of incidence, and f is the focal length. The amount of power scattered into the orthogonal linear polarization is just twice this, or

$$1 - L_{xp}^{-1} = \frac{1}{4}\left(\frac{w}{f}\right)^2 \tan^2(i) \tag{5}$$

A more subtle effect is the squint induced between orthogonal circularly polarized beams. Napier [44] has found that the shift, $\Delta\theta$ relative to the 3-dB beamwidth, θ_{3dB}, is given approximately by

$$\frac{\Delta\theta}{\theta_{3dB}} \approx 0.7 \frac{w}{f} \tan(i) \qquad (6)$$

We see that it is related to the cross-polar power loss by

$$\frac{\Delta\theta}{\theta_{3dB}} \approx 1.4\sqrt{1 - L_{xp}^{-1}} \qquad (7)$$

and a loss of only 0.1 % is associated with a 4 % beam squint.

With several mirrors these effects may be cumulative or tend to cancel, depending on the focal lengths and orientations of the mirrors. In the geometrical optics limit perfect cancellation may be achieved [45] but this may not be the case with quasioptical beams [46]. For the systems considered here the degree of cancellation has been guesstimated.

When the feed is offset laterally from the focus of the Cassegrain antenna, Napier [44] estimates a beam squint of about 1 % per 100 mm offset, which we have verified by geometrical optics calculation.

7.1.6 *Aberrations Due to Phase Center Motion*

Ellipsoidal mirrors are designed to transform a spherical field with its center of curvature at one focus to a field with its center of focus at the other focus. If the input and output are quasi-optical beams, the phase centers at the mirror will generally vary with frequency. At frequencies other than the design center-frequency there will therefore be some aberration of the wavefront. To estimate the associated loss we use the Mathcad document developed by Lazareff [47]. The ellipsoid parameters were calculated for the geometric center of the band, which tends to give equal phase error losses at the band edges. As with the losses in the previous section, contributions from consecutive mirrors may not be directly additive, but here we assume they are since the effects are small.

7.1.7 *Grid Losses*

To estimate ohmic losses for grids we take the effective resistivity to be eight times higher than for the mirrors to account for the wire spacing and material. The Ruze loss is estimated as being twice as large as for the mirrors though it applies only to the reflected polarization. (Since both these losses apply only to the reflected wave the average for the two is given here).

Leakage losses for well-made grids are much less than a percent. They are due to the small shunt capacitance between the wires for the TE field, and to the finite shunt inductance for the TM field. These two leakages have opposite dependences on wire spacing and the optimum occurs for a pitch to diameter ratio of about four [28].

7.2 Degradation Due to Offset Feeds

Any offset of the feed from the optimum focus will degrade sensitivity as a result of aberrations and spillover. These have to be taken into account in the optical design and loss and noise budget.

7.2.1   Aberrations Due to Feed Lateral Offset

The three main aberrations resulting from a lateral feed offset are coma, astigmatism, and curvature. Expressions for these are given in [17], which showed that astigmatism and curvature are much more significant than coma, which may be neglected. Figure 12 shows the maximum feed offsets, which can be tolerated if the efficiency loss is to be less than 1 %.
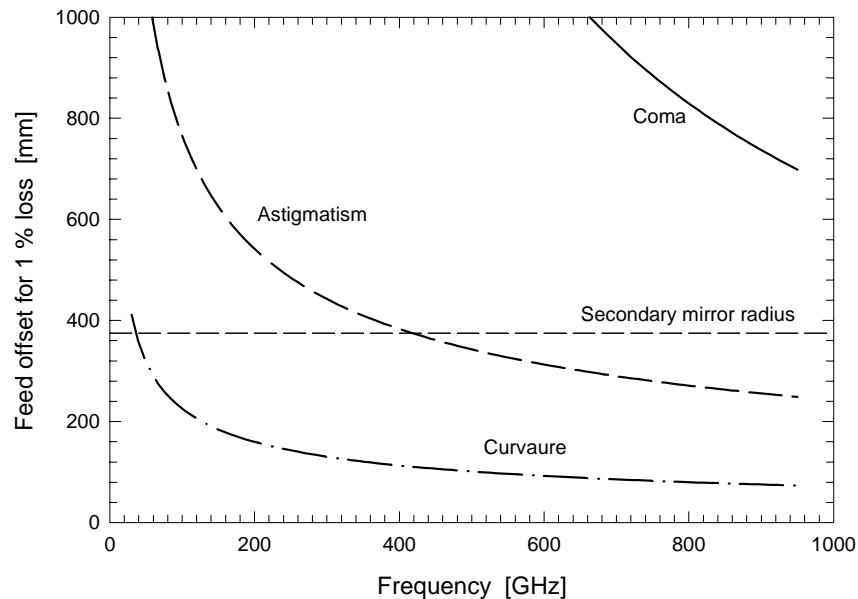

Figure 12. Maximum tolerable feed offset in the focal plane for an efficiency loss of 1 % for the primary aberrations applicable to the ALMA 12-m antennas.

The curvature loss may be almost completely eliminated by refocusing to the Petzval surface, leaving astigmatism as the dominant aberration. In [17] the equation for astigmatism assumed that the feed was located at one of the line foci. In principle the gain can be increased by putting the feed half way between the sagittal and tangential foci, but it turns out that the improvement is small and comparable to the loss from coma and the residual of the curvature. The astigmatism curve in Figure 12 is therefore a good measure of the total aberration offset limit for the ALMA antennas.

At least the prototype antennas, and possibly some or all of the production ones will have nutating secondary mirrors for single-dish measurements. These will introduce additional aberrations. According to Radford [48] the center of rotation will be 215 mm below the prime focus. In this case the aberration is mainly coma [17]. Since coma is orthogonal to astigmatism, the phase errors due to offset feeds and secondary mirror nutation will add in quadrature and the loss in efficiency will be the sum of the two losses. The maximum beam throw will be ±1.5 arcmin which allows a total throw of 3 beamwidths down to about 100 GHz. Coma phase errors are proportional to the beam throw, so the loss is independent of wavelength for a throw of a given number of beamwidths. For ±1.5 beamwidths the loss is about 1 %.

7.2.2   Focus

If the receiver focal point does not coincide with the telescope focus there will be a loss of efficiency due to defocusing. This may be partially recovered by moving the secondary mirror axially. Without refocusing the secondary, the receiver bands would have to have their focal points very close to the nominal focus. Figure 13 gives the maximum axial defocus for a 1 % reduction in efficiency calculated using ray tracing. At 200 GHz the focus location has to be within ~ 40 mm of the nominal Cassegrain focus if the secondary mirror is fixed; the acceptable range for the focus can be increased to ~ 500 mm if refocusing is allowed, as it will be for ALMA. The secondary has to move about 2.8 μm to compensate 1 mm of displacement the feed.

When the axial focus loss is calculated for offset feeds the displacement should be taken from the Petzval surface as discussed in Sec. 7.2.1.
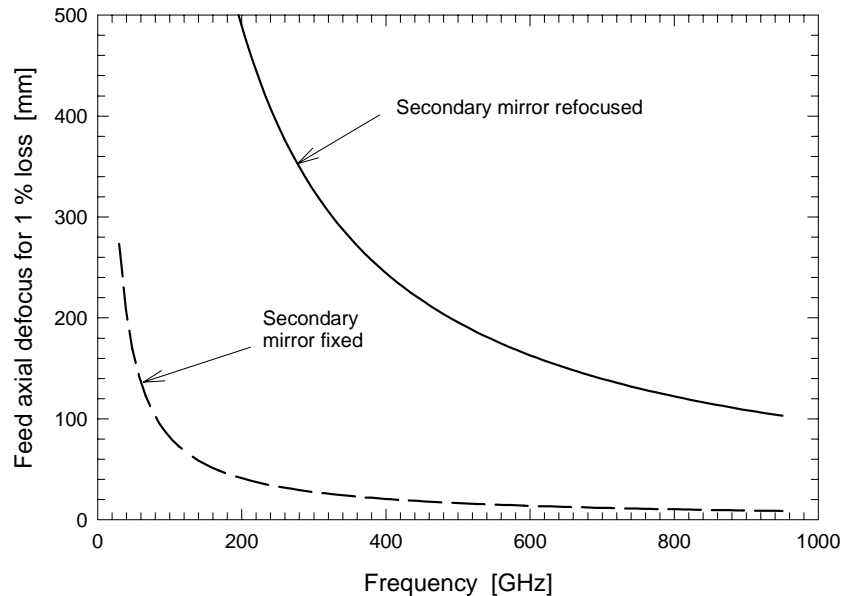

Figure 13. Allowable displacement of feed along antenna axis for <1 % loss of efficiency. The dashed line does not include refocusing the secondary, while the solid one does. The secondary has to move about 2.8 mm per mm of movement of the feed.

7.2.3   Spillover

Offsetting the feed laterally from the focus will cause increased spillover. In the Geometrical Optics approximation all the rays from the feed go to the sky when the feed is on axis, but as the feed is offset, rays at the edge will spill past the primary on to ambient surroundings giving a spillover noise contribution which is roughly linear with offset distance. Diffraction will cause spillover even with on-axis feeds unless the secondary is significantly undersized. The spillover may be calculated using Physical Optics [49]. Figure 14 gives the results for some of these calculations for the ALMA antennas. For an on-axis feed the spillover has the expected $\lambda^{\frac{1}{2}}$ dependence. At low frequencies the on-axis spillover is high but the increase for off-axis feeds is small. Up to about 200 GHz the increase is less than about 1 K. For high frequencies the on-axis

spillover is small but the increase with off-axis distance is larger. However this degradation increases more slowly with off-axis distance than aberrations do, and more slowly with frequency than the quantum noise limit. We can conclude that the effects of spillover noise are a minor consideration in the optical design.
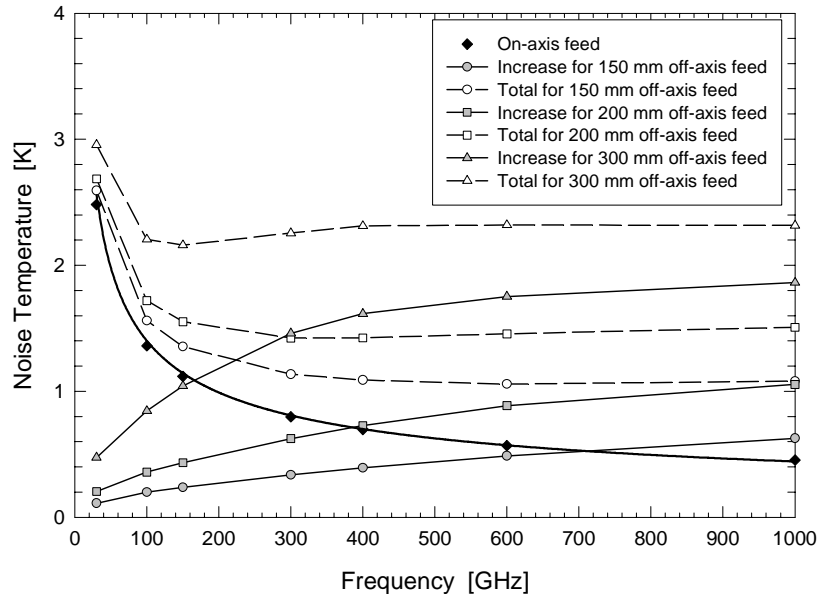

Figure 14. The heavy line shows the noise power received due to diffraction at the secondary when the feed is on axis. The other curves show how much the noise is degraded when the feed is moved off axis.

7.3   Summary of Alignment Tolerances

The elements in the optical train for each band will not be exactly at their design positions because of: fabrication tolerances; dewar deformation under pressure; gravity deformations. The positioning errors will cause:

1. Linear offsets of the coupled beam (reckoned at the Cassegrain focus);
2. Angular offsets of the coupled beam;
3. A distortion of the coupled beam, leading to a loss of aperture efficiency; due to the fact that refocusing elements are exactly stigmatic only for the nominal beam.

These effects have been calculated for the optical trains of the various bands [50]. Among the three effects listed, the first one amounts to a re-definition of the pointing offset for a particular band, which will be calibrated anyway. The second one corresponds to a misalignment of the illumination pattern on the secondary mirror of the telescope[7]; an efficiency loss of 1.3 % corresponds to a misalignment of 10 % of the secondary's radius,

---

[7] A laterally displaced aperture will also cause a phase gradient in the far-field beam pattern. The consequences of this are still under investigation.

or to an angular offset of the coupled beam of 6.25 mrad, with the ALMA antenna geometry. That is the main concern in alignment tolerance. The third effect is not significant at the level of alignment accuracy required by the beam angular alignment.

Linear and angular positioning tolerances have been calculated for each element of the various bands, corresponding to a 6 mrad tolerance on the angle of the coupled beam at the Cassegrain focus. The linear tolerances are 0.2 mm or more, and the angular tolerances are 2 mrad or more.
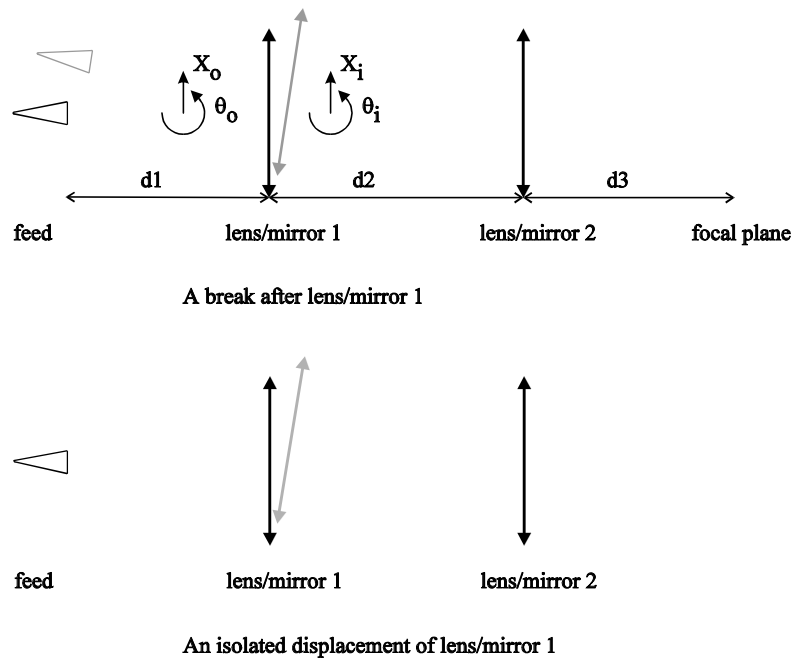

Figure 15. Definition of terms used in tolerance calculations.

What tolerances are reasonably achievable? Following consultation with the IRAM workshop, it appears that, for elements within a compact assembly, like the cold optics of a cartridge, tolerances of 0.02 mm and 0.5 mrad can be achieved. For Bands 1–4, part of the optical train (the horn) is referenced to the cartridge, while the rest (lens, mirrors) is referenced to the front face of the dewar. If the dewar is first assembled (with alignment pins), and then the seating planes for the cartridges (on the rear side) and for the warm optics (on the front side) are machined jointly on a large-capacity machine, relative alignment tolerances of 0.05 mm and 0.2 mrad can be achieved.

Therefore machining accuracies can meet the requirements of alignment. The discussion of thermal and gravity deformation is best left to RAL, who have made detailed simulations of these effects.

7.4   Aperture Efficiency

The total aperture efficiency will depend on several factors not related to the details of the feed. This includes the radiation efficiency (ohmic loss), diffraction efficiency, blockage efficiency, and Ruze (surface error, calculated for $\varepsilon = 20\,\mu m$) efficiency of the primary and secondary antenna mirrors. These are collected in Table IX, along with the illumination and

spillover efficiencies that would result from a perfectly imaged corrugated horn feed as shown in Figure 16.

Figure 16 also plots the efficiency with the receiver optical losses included. In practice the efficiency would not be measured at the feed horn aperture. Some of the receiver optics losses would appear rather as a degradation of the receiver noise temperature.

TABLE IX

ESTIMATED APERTURE EFFICIENCY FOR AN IDEAL FEED SYSTEM WITH A CORRUGATED HORN.

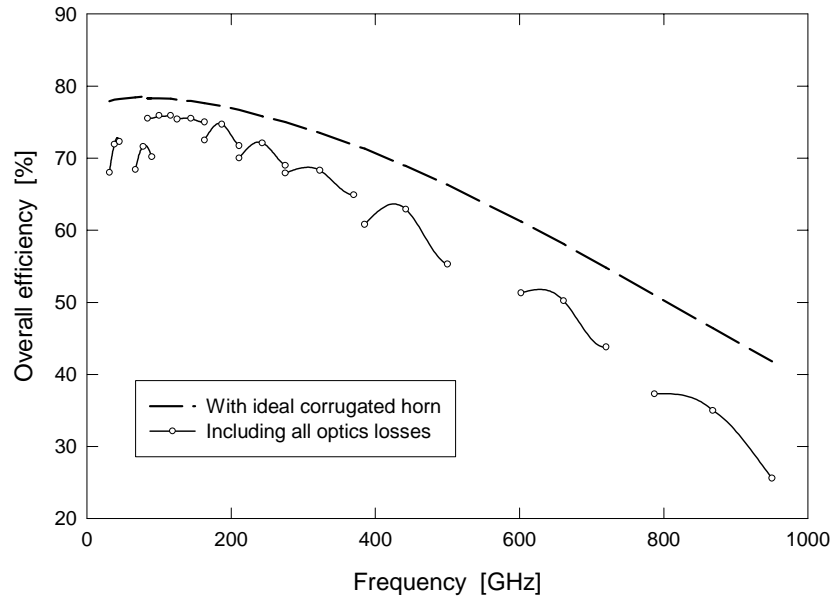| Frequency [GHz]	Radiation efficiency [%]	Illumination efficiency [%]	Spillover efficiency [%]	Diffraction efficiency [%]	Ruze efficiency [%]	Blockage efficiency [%]	Total aperture efficiency [%]
31	99.7	91.1	95.4	96.8	99.9	93.0	77.9
38	99.6	91.1	95.4	97.1	99.9	93.0	78.1
45	99.6	91.1	95.4	97.3	99.9	93.0	78.2
67	99.5	91.1	95.4	97.8	99.7	93.0	78.4
78	99.5	91.1	95.4	98.0	99.6	93.0	78.5
90	99.4	91.1	95.4	98.1	99.4	93.0	78.3
84	99.4	91.1	95.4	98.0	99.5	93.0	78.3
100	99.4	91.1	95.4	98.2	99.3	93.0	78.3
116	99.3	91.1	95.4	98.3	99.1	93.0	78.2
125	99.3	91.1	95.4	98.4	98.9	93.0	78.1
144	99.3	91.1	95.4	98.5	98.6	93.0	77.9
163	99.2	91.1	95.4	98.6	98.2	93.0	77.6
163	99.2	91.1	95.4	98.6	98.2	93.0	77.6
187	99.2	91.1	95.4	98.7	97.6	93.0	77.2
211	99.1	91.1	95.4	98.8	96.9	93.0	76.7
211	99.1	91.1	95.4	98.8	96.9	93.0	76.7
243	99.0	91.1	95.4	98.8	95.9	93.0	75.8
275	99.0	91.1	95.4	98.9	94.8	93.0	75.0
275	99.0	91.1	95.4	98.9	94.8	93.0	75.0
323	98.9	91.1	95.4	99.0	92.9	93.0	73.5
370	98.8	91.1	95.4	99.1	90.8	93.0	71.8
385	98.8	91.1	95.4	99.1	90.1	93.0	71.3
442	98.7	91.1	95.4	99.1	87.2	93.0	68.9
500	98.6	91.1	95.4	99.2	83.9	93.0	66.3
602	98.5	91.1	95.4	99.3	77.5	93.0	61.2
661	98.4	91.1	95.4	99.3	73.6	93.0	58.1
720	98.3	91.1	95.4	99.3	69.5	93.0	54.8
787	98.3	91.1	95.4	99.4	64.7	93.0	51.0
868	98.2	91.1	95.4	99.4	58.9	93.0	46.4
950	98.1	91.1	95.4	99.4	53.0	93.0	41.8

Figure 16. Estimated aperture efficiency. The dashed line shows the expected efficiency if an ideal corrugated horn is perfectly imaged on to the secondary mirror. The solid lines give the calculated efficiency including the optics. This is *not* the efficiency, which would be measured by the normal procedure since it is referred to the aperture of the feed horn which is not accessible for hot and cold load measurements.

7.5   Frequency Bands

For reference the frequency bands for the receivers are given below

TABLE X
FREQUENCY BANDS FOR THE ALMA RECEIVERS.

Band	Lowest frequency [GHz]	Highest Frequency [GHz]	5w at secondary focus [mm]
1	31.3	45	353
2	67	90	165
3	89 (84) [†]	116	124
4	125	163	88
5	163	211	68
6	211	275	52
7	275	370	40
8	385	500	29
9	602	720	18
10	787	950	14

[†]The extension of Band 3 down to 84 GHz is under consideration but all calculations for the optics include this lower limit.

8 References

[1]   J. Lamb, "A possible receiver optics layout for the MMA," NRAO, Millimeter Array Memo Series No. 102, Oct. 1993.

[2]   P. Napier, J. Bieging, J. Cheng, D. Emerson, M. Gordon, M. Holdaway, J. Kingsley, J. Lugten, J. Payne, and D. Woody, "A strawman optics layout for the MMA Antenna," NRAO, Millimeter Array Memo Series No. 163, Oct. 1996.

[3]   J. Lugten and J. Welch, "A suggested receiver layout for the MMA antenna," NRAO, Millimeter Array Memo Series No. 183, Sep. 1997.

[4]   J. Lugten, P. Napier, J. Bieging, J. Cheng, D. Emerson, M. Fleming, M. Holdaway, J. Kingsley, J. Lamb, J. Mangum, J. Payne, W. Welch, and D. Woody, "A strawman optics layout for the MMA antenna-version 2," NRAO, Millimeter Array Memo Series No. 215, Jun. 1998.

[5]   V. Belitsky, "Suggestion on LSA/MMA front-end optical layout," NRAO, Millimeter Array Memo Series No. 242, Jan. 2000.

[6]   W. Grammer, B. Shillue, L. D'Addario, and J. Payne, "Proposal for ALMA front end optics," NRAO, ALMA Memo Series No. 324, Sept. 2000.

[7]   M. Carter, "ALMA Receiver Optics," ESO BCSW: ALMA – Receivers, Jul. 2000.

[8]   A. Wootten, L. Snyder, E. van Dishoeck, and F. Owen, "Frequency band considerations and recommendations," NRAO, ALMA Memo Series No. 213, May 2000.

[9]   "Report of the ALMA Scientifc Advisory Committee: March 2000 Meeting," ALMA Scientifc Advisory Committee (Neal Evans (Chairman), Karl Menten (Vice-Chairman)), Mar. 2000.

[10]   "Minutes of First Joint Receiver Design Group (JRDG) Meeting," NRAO, Tucson, 30 Sep. 1999.

[11]   "Minutes of the second Joint Receiver Design Group (JRDG) Meeting," IRAM Grenoble, 2-3 Dec. 1999.

[12]   R. Hills, J. Richer, H. Smith, V. Belitsky, R. Booth, and D. Urbain, "Development of 183 GHz water vapour radiometers for ALMA," Sept. 2000.

[13]   R. Hills and J. Richer, "Water Vapour Radiometers for ALMA," NRAO, ALMA Memo Series No. 303, Apr. 2000.

[14]   "Summary Report of the Fourth Joint Receiver Design Group (JRDG) Meeting," Cambridge, UK, (J. Payne and W. Wild), 7-8 Sep. 2000.

[15]   "Report of the ALMA Scientific Advisory Committee: September 2000 Meeting," ALMA Scientific Advisory Committee, (K. Menten (Chairman), J. Welch (Vice-Chairman)), 10 Oct. 2000.

[16]   M. Harman, B. Ellison, T. Bradshaw, and A. Orlowska, "ALMA receiver cartridge thermal link," 17 May 2000.

[17]   J. W. Lamb, "Optimized optical layout for MMA 12-m antennas," NRAO, ALMA Millimeter Array Memo Series No. 246, Jan. 1999.

[18]   T.-S. Chu, "An imaging beam waveguide feed," *IEEE Trans Antennas and Propagat.*, vol. AP-31, no. 4, pp. 614–619, Jul. 1983.

[19]   J. W. Lamb, "Optical study for ALMA receivers," NRAO, ALMA Memo Series No. 359, Mar. 2001.

[20]   J. W. Lamb, "ALMA evaluation receiver optics design," OVRO-ALMA Design Report, Apr. 2000.

[21]   J. W. Lamb, "Cross-polarization and astigmatism in matching grooves," *Int. J. IR and Millimeter Waves*, vol. 17, no. 12, pp. 2159–2165, Dec. 1996.

[22]   P.-S. Kildal, "Meniscus-lens-corrected corrugated horn: a compact feed for a Cassegrain antenna," *IEE Proc. Part H*, vol. 131, no. 6. pp. 390-394, Dec. 1984.

[23]   J. W. Lamb, "Infrared filters for cryogenic millimeterwave receivers," *Int. J. Infrared and Millimeter Waves*, vol. 14, no. 5, pp. 959-967, 1993.

[24]   R. Padman, "Reflection and cross-polarisation properties of grooved dielectric panels," *IEEE Trans. Antennas Propagat.*, vol. AP-26, no. 5, pp. 741–743, Sep. 1978.

[25]   J. Clarke and L. D'Addario, "Tests of materials for use in multi-layer infrared filters in cryogenic applications," NRAO, ALMA Memo No. 269, Jul. 1999.

[26]   D. J. Benford, M. C. Gaidis, and J. W. Kooi, "Transmission properties of Zitex in the infrared to the submillimeter," in *Proc. Of the 10th Int. Symp. On Space THz Tech*. (T. Crowe, ed.), pp. 405–413, 1999.

[27] F. Sobel, F. L. Wentworth and J. C. Wiltse, "Quasi-optical surface waveguide and other components for 100 to 300 Gc region," *IRE Trans. Microwave Theory Tech.*, vol. MTT-9, no. 6, pp. 512-518, Nov. 1961.

[28] T. Larsen, "A survey of the theory of wire grids," *IRE Trans. Microwave Theor. Tech.*, vol. MTT-10, pp. 191–201, May 1962.

[29] Y. Sekimoto, J. Inatani, T. Noguchi, K. Kohno, H. Iwashita, R. Kawabe, S. Yokogawa, and T. Sakai, "A Japanese plan of receiver developments for LMSA/ALMA," NRAO, ALMA Memo No. 315, Jun. 2000.

[30] J. R. Birch, J. D. Dromey and J. Lesurf, "The optical constants of some common low-loss polymers between 4 and 40 cm^{-1}," *Infrared Phys.*, vol. 21, pp. 225-228, 1981.
(For numerical data, see also: J. R. Birch, J. D. Dromey and J. Lesurf, "The optical constants of some common low-loss polymers between 4 and 40 cm^{-1}," NPL Report DES 69, National Physical Laboratory (UK), Feb. 1981).

[31] Y Sekimoto, private communicaton.

[32] A. Baryshev and W. Wild, "Band 9 optical layout," NOVA/SRON, Dec. 2000.

[33] H. van de Stadt, Private communication.

[34] "Minutes of Joint Receiver Design Group (JRDG) Monthly Teleconference," May, 2000.

[35] H. Riewaldt, "Basic antenna definitions," NRAO, ALMA-US ICD No. 11, Jan. 2000.

[36] J. Ibruegger, "Transmission of room-temperature radiation by materials at low temperatures," *Int. J. IR and Millimeter Waves*, vol. 5, no. 5, May 1984.

[37] S. Navarro, Private communication.

[38] J. W. Lamb and D. Woody, "Radiometric correction of anomalous refraction," ALMA Millimeter Array Memo Series, No. 224, Aug. 1998.

[39] A. J. Gatesman, R. H. Giles, and J. Waldman, "High-precision reflectometer for sub-millimeter wavelengths," *J. Opt Soc. Am. B*, vol. 12, no. 2, pp. 212–219, Feb. 1995.

[40] M. Born and E. Wolf, *Principles of Optics*, Oxford: Pergamon Press, 1980.

[41] J. W. Lamb, "Miscellaneous data on materials for millimeter and submillimeter optics", *Int. J. IR and Millimeter Waves*, vol. 17, no. 12, pp. 1997–2034, Dec. 1996.

[42] J. W. Flemming and G. W. Chantry, "Accurate radiometric measurements on low-loss polymers at submillimetric wavelengths," *IEEE Trans. Instrum. Meas.*, vol. IM-23, no. 4, pp. 473-478, Dec. 1974.

[43] J. A. Murphy, "Distortion of a simple Gaussian beam on reflection from off-axis ellipsoid mirrors," *Int. J. Infrared and Millimeter Waves*, vol. 8, no. 9, pp. 1165–87, 1988.

[44] P. J. Napier, Private communication.

[45] C. Dragone, "Offset antennas with perfect pattern symmetry and polarization discrimination," *Bell System Tech. J.*, vol. 57, no. 7, pp. 2663-2684, Sep. 1978.

[46] T.-S. Chu, "Polarization properties of offset dual-reflector antennas," *IEEE Trans. Antennas and Propagat.*, vol. 39, no. 12, pp. 17531756, Dec. 1991.

[47] B. Lazareff, "Conic mirror used in vicinity of geometrical focus," Mathcad document, IRAM, 6 Apr. 1993.

[48] S. J. Radford, Private Communication, 2 Oct. 2000.

[49] W. V. T. Rusch, "Scattering from a hyperboloidal reflector in a Cassegrainian feed system," *IEEE Trans. Antennas Propagat.*, vol. AP-11, no. 4, pp. 414-421, July 1963.

[50] B. L. Lazareff, "Alignment tolerances for ALMA optics, Version 1.9," Nov. 2000.